

# Whole transcriptome analysis on blue light-induced eye damage

Xin-Li Ouyang<sup>1</sup>, Bo-Yu Chen<sup>2</sup>, Yong-Fang Xie<sup>1</sup>, Yi-De Wu<sup>1</sup>, Shao-Jia Guo<sup>1</sup>, Xiao-Yun Dong<sup>1</sup>, Guo-Hui Wang<sup>1</sup>

<sup>1</sup>Key Laboratory of Biological Medicines in Universities of Shandong Province, Weifang Medical University, Weifang 261053, Shandong Province, China

<sup>2</sup>Shijiazhuang Aier Eye Hospital, Bethune International Peace Hospital of PLA, Shijiazhuang 050082, Hebei Province, China

**Co-first authors:** Xin-Li Ouyang, Bo-Yu Chen, and Yong-Fang Xie

**Correspondence to:** Guo-Hui Wang and Xiao-Yun Dong. Key Laboratory of Biological Medicines in Universities of Shandong Province, Weifang Medical University, Weifang 261053, Shandong Province, China. wangguohui1983@163.com; dongxiaoyun377400@wfmuc.edu.cn

Received: 2020-03-30 Accepted: 2020-05-07

## Abstract

• **AIM:** To analyze abnormal gene expressions of mice eyes exposed to blue light using RNA-seq and analyze the related signaling pathways.

• **METHODS:** Kunming mice were divided into an experimental group that was exposed to blue light and a control group that was exposed to natural light. After 14d, the mice were euthanized and their eyeballs were collected. Whole transcriptome analysis was attempted to analyze the gene expression of the eyeballs using RNA-seq to reconstruct genetic networks. Gene Ontology (GO) and Kyoto Encyclopedia of Genes and Genomes (KEGG) analysis were used to reveal the related signaling pathways.

• **RESULTS:** The 737 differentially expressed genes were identified, including 430 up and 307 down regulated genes, by calculating the gene FPKM in each sample and conducting differential gene analysis. GO and KEGG pathway enrichment analysis showed that blue light damage may associated with the visual perception, sensory perception of light stimulus, phototransduction, and JAK-STAT signaling pathways. Differential lncRNA, circRNA and miRNA analysis showed that blue light exposure affected pathways for retinal cone cell development and phototransduction, among others.

• **CONCLUSION:** Exposure to blue light can cause a certain degree of abnormal gene expression and modulate

signaling pathways in the eye.

• **KEYWORDS:** blue light; eye; whole transcriptome sequencing; gene expression; signaling pathways; mice

**DOI:10.18240/ijo.2020.08.06**

**Citation:** Ouyang XL, Chen BY, Xie YF, Wu YD, Guo SJ, Dong XY, Wang GH. Whole transcriptome analysis on blue light-induced eye damage. *Int J Ophthalmol* 2020;13(8):1210-1222

## INTRODUCTION

Exposure to blue light induces various biochemical and physiological changes in the eyes. In previous studies, blue light has been found to have high photochemical energy, and long exposure times to this high energy light often lead to eye diseases such as age-related maculopathy, dry eye and cataracts<sup>[1-5]</sup>, and it will cause a worsening of visual fatigue and nearsightedness<sup>[6-7]</sup>. In addition, blue light can affect sleep quality by inhibiting melatonin secretion and affecting the hormonal balance<sup>[8-11]</sup>. It has been reported that the blue light spectral range at 415-455 nm was the most damaging light to the retina; light could pass through the lens directly to the retina and lead to irreversible photochemical retinal damage<sup>[12-16]</sup>. Moderately intense blue light can induce non-necrotic cell death or apoptosis and high intensity blue light can induce necrosis due to its phototoxicity<sup>[17-19]</sup>. The mechanism underlying this damage is suggested to be related to the accumulation of reactive oxygen species (ROS) and oxidative stress<sup>[20-21]</sup>. Additionally, in rat retina, blue light-induced mitochondrial dysfunction was observed<sup>[22-24]</sup>.

In addition to the effects on the function and structure of the eyes, some data also suggest that periodic blue light exposure can affect gene expression. Genetic studies suggest that prolonged exposure to blue light can increase Bax and decrease Bcl-2 and Bcl-xL expression<sup>[25]</sup>. Blue light induces a large number of free radicals that can destroy messenger ribonucleic acid (mRNA) and proteins under aerobic conditions, and it has been unequivocally demonstrated that the N-retinylidene-N-retinylethanolamine (A2E) is a mediator of blue light damage in the retinal pigment epithelium<sup>[26-29]</sup>.

In recent years, people have become increasingly attentive to eye discomfort related to blue light. Previous studies provided a solid framework for future eye disease studies and the development of blue light blocking filters. These studies revealed the important influence of blue light on the function and structure of the eyes; however, the cellular and molecular mechanisms leading to blue light-induced retinal damage are not completely understood. To understand the molecular mechanisms associated with blue light-induced eye diseases, we hypothesized that gene expression would change in rat eyeballs exposed to experimental blue light compared to normal eyeballs. To test the hypothesis, we investigated the whole-genome regulation of eyeballs exposed to blue light. We systematically analyzed the genetic background of blue light-exposed eyeballs using genome-wide gene expression profiling (RNA-seq). Using gene-based analysis, we identified differentially expressed RNA and identified genes that are involved in blue light hazards. We found that blue light influenced the expression of genes in the eyeballs and modulated a set of signaling pathways to cause eye diseases.

## MATERIALS AND METHODS

**Ethical Approval** All protocols were approved by the Laboratory Animal Ethics Committee of Weifang Medical University and the study was adherence to the ARVO Statement for the Use of Animals in Ophthalmic and Vision Research.

**Animals and Processing Methods** Specific pathogen free (SPF), 4-week-old female Kunming mice (20±0.1 g) were obtained from the Jinan Pengyue experimental animal company [SCXK (Lu) 20140007, Jinan, China]. The mice were housed at 25°C and fed standard rodent chow and tap water. The mice were housed for 2d before experiments to adapt to the environment. A total of 5 mice were separated and housed in two groups. The control group was exposed to natural light, while the experimental group was exposed to blue light (18 W, PL-L, Philips) and surrounded by a dark container. After 14d, the mice were euthanized and their eyeballs were collected in phosphate buffer saline (PBS; pH=7.5) for subsequent whole transcriptome analysis by Genesky Bio-Tech (Shanghai, China). All data had been deposited at NCBI Gene Expression Omnibus (<http://ncbi.nlm.nih.gov/geo/>) and the GEO accession number is GSE149549.

**Total RNA Extraction and Quality Control** Total RNA was extracted from each tissue sample using the Trizol method. The total amount and concentration of the RNA was measured using an Invitrogen Qubit 3.0 spectrophotometer (Thermo Fisher Scientific, USA). The purity of the RNA was confirmed by testing the ratio of OD 260/280 and OD 260/230 using a NanoDrop 2000. The integrity of the RNA was measured by agarose gel electrophoresis and an Agilent 2100 bioanalyzer.

RNA samples with concentrations  $\geq 100$  ng/ $\mu$ L, total RNA  $> 2$   $\mu$ g, OD 260/280 values between 1.8 and 2.2, OD 260/230  $\geq 2.0$ , and RNA integrity (RIN) values  $\geq 7$  were considered qualified RNA samples.

## Total RNA-seq Library Preparation and Quality Control

After incubation of RNA with a biotin-modified probe, the probe was captured by a streptavidin magnetic bead to eliminate rRNA. The obtained samples were purified by AMPure XP magnetic beads, and then buffer composed of elution, fragmented, and random primers was added and the samples were incubated at 94°C. Thermal fracture led to fragments distributed between 100 and 300 bp. Using first-strand synthesis buffer and Invitrogen SuperScript IV reverse transcriptase (SS IV; Thermo Fisher Scientific, USA), this fragmented RNA was used as a template to synthesize the first-strand cDNA. Actinomycin D was added to the first-strand synthesis buffer to prevent the reverse transcription of DNA templates and to ensure the reverse transcription specificity of RNA templates. After that, the double-stranded synthesis premix system was added to the synthesized first-strand cDNA, and the product was purified by Agencourt AMPure XP magnetic beads. From this reaction we obtained purified double-stranded cDNA and then added a 3' end plus "A" buffer reaction system to this system. Finally, ligation buffer and a double-stranded sequencing linker was added to the library; we used T4 DNA ligase (NEB, UK; 30°C, 10min) to attach the illumina sequencing linker to the DNA library. The library was purified using the Agencourt SPRI select Nucleic Acid Fragment Screening kit (Beckman Coulter, USA).

We used polymerase chain reaction (PCR) to expand the cDNA library, the Invitrogen Qubit 3.0 spectrophotometer (Thermo Fisher Scientific, USA) to measure the library concentration, and the Agilent 2100 bioanalyzer to measure the library fragment sizes and distribution. After diluting qualified samples, the library was sequenced using the illumina high-throughput sequencing platform and a 2×150 bp paired-end sequencing strategy.

## Small RNA Library Construction and Quality Control

Total RNA extraction and quality control are described in section 1.2. Purified total RNA was ligated to the 3' end (T4 DNA ligase 2; 28°C, 60min) and 5' end (T4 RNA ligase; 28°C, 60min) of mature miRNA. Using Super Script IV reverse transcriptase, first-strand cDNA was synthesized using reverse transcription primers complementary to the sequence on the linker. We performed PCR synthesis that used the first-strand cDNA as a template to expand the miRNA double-stranded library. The target miRNA library was separated using high-resolution polyacrylamide gel electrophoresis (PAGE, 6%). The cDNA library concentration was measured using the Invitrogen Qubit 3.0 spectrophotometer (Thermo

Fisher Scientific, USA). Library fragment size and distribution were measured using an Agilent 2100 bioanalyzer. After the qualified sample was diluted, the library was sequenced by 2×150 bp paired-end sequencing using an illumina high-throughput sequencing platform.

**Sequencing Data Quality Control, Filtration, and Reference Genome Alignment** The raw sequencing data was quality control tested using Fast QC and R (<http://www.bioinformatics.babraham.ac.uk/projects/fastqc/>). Raw reads were filtered using TrimGalore ([http://www.bioinformatics.babraham.ac.uk/projects/trim\\_galore/](http://www.bioinformatics.babraham.ac.uk/projects/trim_galore/)) to remove the sequencing primer, sequences with low end mass ( $Q < 10$ ) and sequences with fragment lengths  $< 35$  bp. The clean reads were used for subsequent analysis. The filtered reads were compared with the reference database (mouse genome version: mm version) using the HISAT2 software<sup>[30]</sup>. RNA\_seQc (<http://www.broadinstitute.org/cancer/cga/rna-seq>)<sup>[31]</sup> was used to determine regional distribution statistics for exons, introns and intergenic (gene) regions. The saturation and redundancy sequences of samples were analyzed and measured using the RNA\_seQc software. Variable shear analysis was performed using rMATS<sup>[32]</sup>. Transcripts of each sample were assembled and merged and new transcripts were predicted using StringTie and cufflink.

**RNA (lncRNA, mRNA, circRNA) expression and differential analysis** The quality-controlled sequences were compared to the reference genome using HISAT2. The expression of known genes and transcripts was quantified using the Stringtie analysis process, and the fragments per kilobase of exon per million fragments mapped (FPKM) values of each RNA at the RNA level were counted. We then compared the RNA expression levels (FPKM value) of the different sample groups using Deseq2 software<sup>[33]</sup>. Differentially expressed RNA (including lncRNA, mRNA, and circRNA) were identified with  $P$  values  $< 0.05$  and  $|\log_2(\text{fold change})| \geq 1$ . RNA with  $\log_2(\text{fold change})$  values  $> 1$  were labeled as upregulated genes (up) and those with  $\log_2(\text{fold change})$  values  $< -1$  were labeled as downregulated genes (down). Differentially expressed RNAs were displayed using a volcano map, and selected differentially expressed RNAs were analyzed using a heatmap.

**Functional and pathway enrichment analysis of differential mRNA** Using the R package clusterProfiler (<http://bioconductor.org/packages/release/bioc/html/clusterProfiler.html>), we obtained the cellular component (CC), molecular function (MF), and biological process (BP) terms of the differentially expressed genes. Enrichment and signaling pathway analysis were performed for differential genes. We used the Kyoto Encyclopedia of Genes and Genomes (KEGG) public database<sup>[34]</sup> for KEGG pathway enrichment analysis

and selected the pathways associated with the differentially expressed genes. The threshold for the above analysis was set to a  $P$ -value  $< 0.05$  and a corrected  $P$ -value ( $P_{\text{adjust}}$ )  $< 0.05$  using the Benjamini and Hochberg method.

**Prediction and functional analysis of differentially expressed lncRNA target genes** LncRNA software<sup>[35]</sup> was used to predicted the target genes of the differentially expressed lncRNA. GO and KEGG pathway enrichment analyses were performed on the differentially expressed lncRNA target genes. The threshold for the above analysis was set to a  $P$ -value  $< 0.05$  and a corrected  $P$ -value ( $P_{\text{adjust}}$ )  $< 0.05$  using the Benjamini and Hochberg method.

**circRNA recognition and analysis** The start and end positions of circRNAs and the gene annotations for the corresponding sources were predicted and statistical analysis was performed on the length of the circRNA using CIRI2 software<sup>[36]</sup>. The expression of circRNAs in different samples was measured by CIRC software. Differential analysis of the circRNA was performed using the R packages clusterProfiler and DEseq<sup>[37-38]</sup>. The standard for differentially expressed circRNAs was  $P < 0.05$  and  $|\log_2(\text{fold change})| > 0$ ; among the differentially expressed circRNAs, a  $\log_2(\text{fold change}) > 0$  was labeled as an upregulated gene (up) and  $\log_2(\text{fold change}) < 0$  was labeled as a downregulated gene (down). The differentially expressed circRNA-derived genes were subjected to GO and KEGG enrichment analysis using the R package clusterProfiler. The significance threshold was set to a  $P$ -value  $< 0.05$  and a Benjamini and Hochberg method-corrected  $P$ -value ( $P_{\text{adjust}}$ )  $< 0.05$ .

**Target miRNA prediction of differential circRNA** The sequences of differentially expressed circRNAs were used to predict miRNA binding sites using miRanda software<sup>[39]</sup>. The miRNA sequence could then be extracted from the miRBase (<http://www.mirbase.org/>) database<sup>[40-43]</sup>.

**miRNA data analysis** Quality control of raw data was carried out using FASTX-Toolkit software ([http://hannonlab.cshl.edu/fastx\\_toolkit/](http://hannonlab.cshl.edu/fastx_toolkit/)), including the filtering out of connector sequences, sequences without a 3' linker and insert, sequences with a Q20 with a ratio below 60% and sequences with lengths other than 18-36 bp. Small RNA length distribution statistics were determined for quality-controlled sequences. The sequences after quality control were BLAST compared (<http://blast.ncbi.nlm.nih.gov/>) with the mature miRNA sequences of the corresponding species from the miRBase database (<http://www.mirbase.org/>)<sup>[40-43]</sup>. All preprocessed and unduplicated unique sequences for each sample were compared with the Rfam database (<http://rfam.xfam.org/>)<sup>[44]</sup>. The number and proportion of sequences for different types of small RNA (such as miRNA, rRNA, scRNA, snoRNA, snRNA, tRNA, etc.) genomes were statistically analyzed.

**Table 1 Summary of RNA-seq data**

Sample	Raw reads	Clean reads	Ratio (%)	GC (%)	rRNA reads	rRNA (%)	Mapped ratio (%)	Intragenic (%)	Exonic (%)	Intronic (%)	Intergenic (%)
14d-B-A	185930276	185876760	99.97	47.10	2614060	1.41	90.28	91.97	37.29	54.68	7.96
14d-B-B	142287612	142238592	99.97	50.18	6951077	4.89	86.52	90.76	40.88	49.88	9.17
14d-L-A	162549728	162486404	99.96	49.07	6046820	3.72	87.95	91.58	40.57	51.01	8.36
14d-L-B	172148134	172091260	99.97	48.77	4908356	2.85	88.98	91.66	38.75	52.91	8.27
14d-L-C	155837534	155792718	99.97	50.00	7356808	4.72	85.93	91.07	39.82	51.25	8.86
Total	780.82 M	780.57 M	/	/	26.56 M	/	/	/	/	/	/
Average	156.16 M	156.11 M	99.97	49.02	5.32 M	3.52	87.93	91.41	39.46	51.95	8.52

**Analysis of miRNA differential expression** The small RNA sequences of all samples were compared with the precursor and mature miRNAs from the miRbase database (<http://www.mirbase.org/>)<sup>[40-43]</sup> of the corresponding species using miRDeep2 software (<https://www.mdc-berlin.de/8551903/en/>)<sup>[45]</sup>, from which we obtained known miRNAs and their secondary structures. The expression of known miRNAs in each sample was statistically analyzed and the expression of new miRNAs in each sample was predicted. Differentially expressed miRNAs were screened using the R package DESeq2<sup>[37-38]</sup>. The screening criteria was  $P < 0.05$  and  $|\log_2(\text{fold change})| > 0$ ;  $\log_2(\text{fold change}) > 0$  was labeled as an upregulated gene (up), and a  $\log_2(\text{fold change}) < 0$  was labeled as a downregulated gene (down). Differentially expressed miRNAs were displayed using a volcano map, and hierarchical clustering analysis (heatmap) was performed on selected differentially expressed miRNAs. The miRNA target genes were predicted using miRanda (<http://www.microrna.org/microrna/home.do>)<sup>[46]</sup> and RNAhybrid (<http://bibiserv.techfak.uni-bielefeld.de/rnahybrid/>)<sup>[47]</sup>. Genes predicted by both methods were reported as the final result. The target genes of differentially expressed miRNAs were subjected to GO and KEGG enrichment analysis. The significance threshold was set to a  $P$ -value  $< 0.05$  and a Benjamini and Hochberg method corrected  $P$ -value ( $P_{\text{adjust}}$ )  $< 0.05$ .

**Coexpression Analysis**

**Differential mRNA-miRNA and lncRNA-miRNA coexpression analysis** The target genes of the differentially expressed miRNAs were predicted using miRanda software, from which we obtained the intersection between predicted target genes and differentially expressed mRNAs. The correlation between differentially expressed mRNAs and miRNAs was tested using the cor. test function in R, with a correlation coefficient  $\text{cor} < 0$ . Similarly, the interaction between lncRNA and miRNA was predicted using miRanda software, and the target relationship between lncRNA and mRNA (cis and trans) was predicted using miRanda software. The intersection of target relationship analysis and coexpression analysis was reported as the final result, and the cor. test

function was used to perform a correlation test. The correlation test standard between lncRNA and differential mRNA expression was  $\text{cor} \neq 0$  and  $P < 0.05$ .

A positive correlation between lncRNA-mRNA expression ( $\text{cor} > 0$  and  $P < 0.05$ ) was constructed for the above relationship, and a lncRNA-miRNA-mRNA ceRNA regulatory network was constructed. The miRNAs with the most ceRNA network regulation were selected to construct ceRNA regulatory maps using Cytoscape software.

**Coexpression analysis of differential circRNA-miRNA and miRNA-mRNA**

Same as above, the target relationship between differentially expressed circRNAs and miRNAs was predicted using miRanda software. The target relationship between differentially expressed mRNAs and miRNAs was predicted using miRanda software and RNAhybrid software. A correlation test was performed using the cor. test function. Based on positive correlations between differentially expressed circRNAs and mRNAs ( $\text{cor} > 0$  and  $P < 0.05$ ), we constructed a circRNA-miRNA-mRNA ceRNA regulatory network and selected the miRNAs with the most ceRNA network regulation for the construction of ceRNA regulatory maps (Cytoscape software).

**RESULTS**

**Summary of Whole-Transcriptome Sequencing Results**

Whole genome sequencing produced a total of 780.82 M raw read (112.41 G bases) data. After filtering and quality control, we obtained 780.57 M reads (112.23 G bases), with an average of 156.11 M reads and 22.45 G bases per sample; the overall sample had an average GC content of 49.02%. The total amount of rRNA was 26.56 M reads which made up an average content of 3.52% of clean reads (Table 1). The above data indicates that we obtained high quality RNA-seq data. The average alignment rate with the reference genome (mm 10 version) was 87.93%, and the alignment rates at intragenic, exonic, intronic, and intergenic regions were 91.41%, 39.46%, 51.95%, and 8.52%, respectively. Saturation analysis of the sequencing results showed that the sequencing results were close to saturation at a 40% alignment of the sequencing reads (the vertical axis value approached 1), indicating that

the overall quality of saturation is high, and the sequencing coverage encompassed most of the expressed genes (Figure 1). **Screening and Enrichment Analysis of Differential mRNAs** By calculating the gene FPKM in each sample and conducting differential gene analysis [using  $P < 0.05$  and  $|\log_2(\text{fold change})| \geq 1$  as the threshold], we identified 737 differentially expressed genes, including 430 upregulated genes [ $\log_2(\text{fold change}) > 1, P < 0.05$ ] and 307 downregulated genes [ $\log_2(\text{fold change}) < -1, P < 0.05$ ; Figure 2A]. These differentially expressed genes had significantly different expression patterns in the case and control samples (Figure 2B).

GO enrichment analysis revealed case/control differential gene enrichment of 425 BP, 29 CC, and 39 MF. The top 30 GO terms are listed in Figure 3A. BPs that were significantly associated with these differentially expressed genes included visual perception/sensory perception of light stimulus and the response to interferon-gamma (IFN- $\gamma$ ). CCs that were significantly associated with these genes included the photoreceptor outer segment, photoreceptor cell cilium, and the non-motile cilium. MFs that were significantly associated included cytokine receptor activity, G-protein coupled receptor binding, CCR chemokine receptor binding and T cell receptor binding ( $P_{\text{adjust}} < 0.05$ ). Further analysis of KEGG pathway enrichment showed that the case/control differentially expressed genes were significantly associated with 39 KEGG pathways, including phototransduction, the JAK-STAT signaling pathway, cytokine-cytokine receptor interactions, chemokine signaling pathways and several pathways associated with viruses or bacteria (including herpes simplex infection, *Staphylococcus aureus* infection, Kaposi sarcoma-associated herpesvirus infection, and Epstein-Barr virus infection, among others). The top 10 KEGG pathways are illustrated in Figure 3B. In addition, we identified 1229 novel transcripts (data not shown) and 207 fusion genes. Many genes in this cluster were involved in the visual perception of light stimulus and phototransduction and included JAK-STAT signaling pathway-associated genes, *OLFM2*, *GUCA1B*, *IRF7*, *MYO10*, and *GADD45B* genes.

**Screening and Analysis of Differentially Expressed lncRNA, circRNA and miRNAs** A total of 4331 differentially expressed lncRNAs were identified in this study, which included 2476 upregulated [ $\log_2(\text{fold change}) > 1, P < 0.05$ ] lncRNAs and 1855 downregulated [ $\log_2(\text{fold change}) < -1, P < 0.05$ , Figure 4A] lncRNAs. Heatmaps of differentially expressed lncRNA clusters showed that these lncRNAs had significantly different expression in the case and control samples (Figure 4B); however, no novel differentially expressed lncRNA was detected. A total of 176 target genes of 169 differentially expressed lncRNAs were predicted using lncTar software. These target genes were significantly enriched

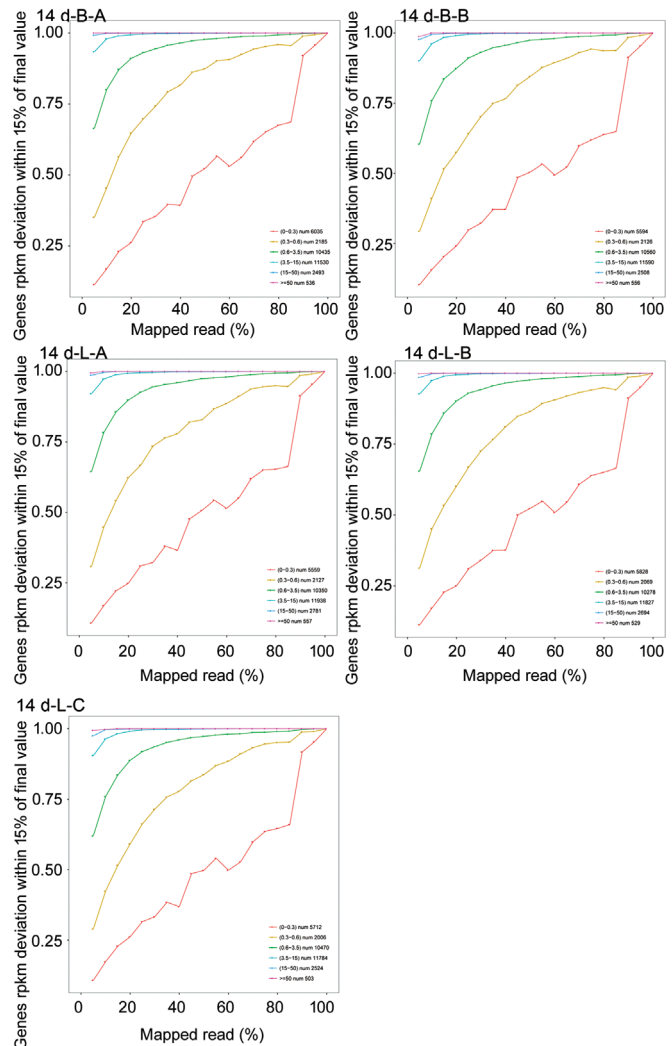


Figure 1 The saturation curves of samples sequenced.

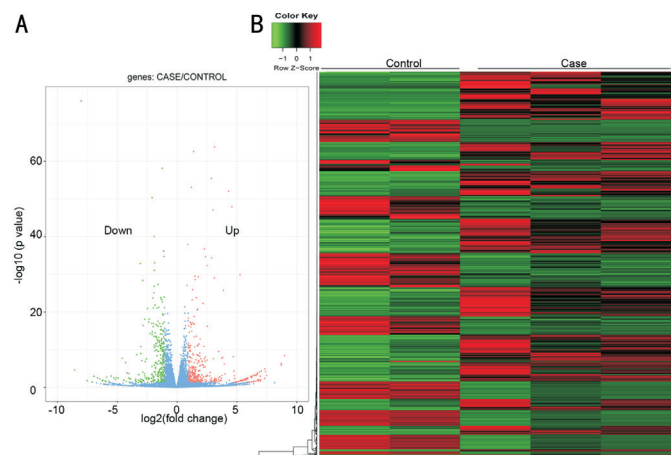
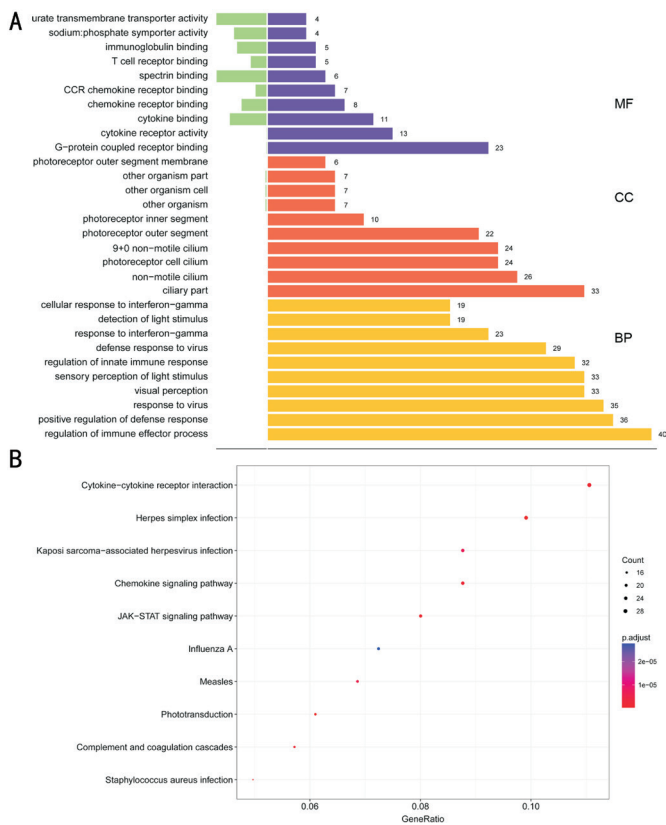
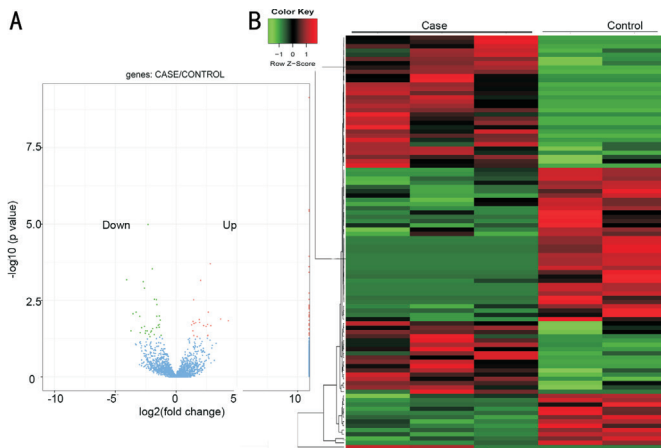


Figure 2 Volcano plot (A) and hierarchical clustering (B) of differentially expressed mRNAs A: Volcano plot. Green and red nodes indicate down- [ $\log_2(\text{fold change}) < -1, P < 0.05$ ] and upregulated mRNAs [ $\log_2(\text{fold change}) > 1, P < 0.05$ ], respectively. Blue color represents nondifferentially expressed mRNAs. B: Heatmap analysis. Red and green color denotes up- and down-regulated expression profiles, respectively.

in 18 GO\_BPs ( $P_{\text{adjust}} < 0.05$ ). GO\_CCs and GO\_MFs that were significantly associated with these target genes were not



**Figure 3** The GO terms and KEGG pathways associated with differentially expressed mRNAs in the case sample compared to the control A: Top 30 GO terms. Ten categories are listed for each classification. B: Top 10 KEGG pathways. Bubble size represents gene number; Bubble color indicates *P*.adjust value. MF: Molecular function; CC: Cellular component; BP: Biological process.



**Figure 4** Volcano plot and hierarchical clustering of differentially expressed lncRNAs A: Volcano plot. Green and red nodes indicate down- [ $\log_2(\text{fold change}) < -1, P < 0.05$ ] and upregulated lncRNAs [ $\log_2(\text{fold change}) > 1, P < 0.05$ ], respectively. Blue color represents nondifferentially expressed lncRNAs. B: Heatmap analysis of differentially expressed lncRNAs. Red and green color denotes up and downregulated expression profiles in samples, respectively.

detected. The top 30 GO terms (10 BP, 10 CC and 10 MF) that were associated with these target genes are displayed in Figure 5A. The GO\_BP terms that lncRNA target genes were

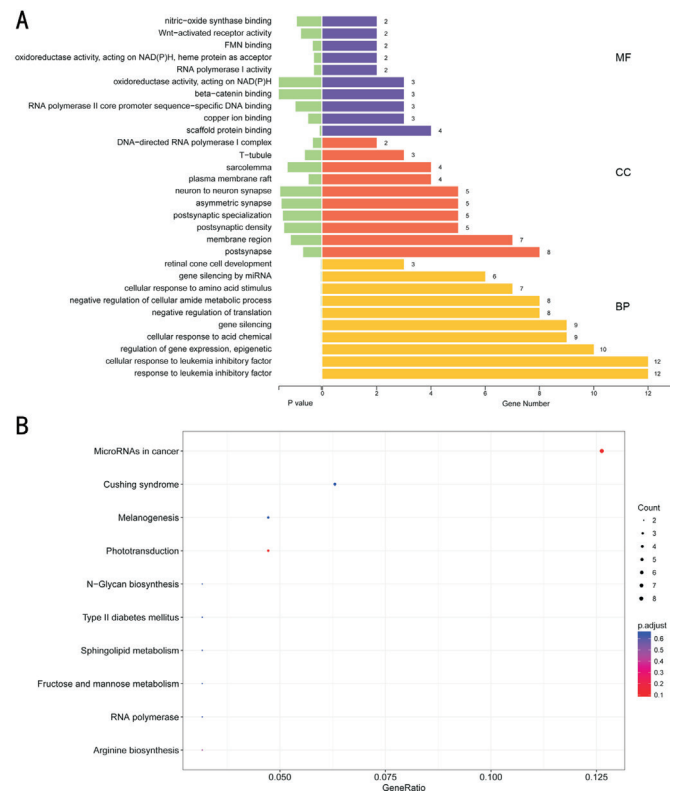


**Figure 5** The GO terms and KEGG pathways associated with the targets of differentially expressed lncRNAs in the case sample compared with the control A: Top 30 GO terms. Ten categories are listed for each classification; B: Top 10 KEGG pathways. Bubble size represents gene number. Bubble color indicates *P*.adjust value. CC: Cellular component; MF: Molecular function; BP: Biological process.

**Table 2** Summary of circRNA prediction

Sample	Count	Max length	Min length	Average length
14d-B-A	3550	196044	142	21975
14d-B-B	2497	199551	140	23091
14d-L-A	2345	199551	137	22541
14d-L-B	2843	192744	135	21888
14d-L-C	2255	191928	143	22026
Average	2698	/	/	22304

associated with included the response to leukemia inhibitory factor, the ‘regulation of gene expression, epigenetic’, retinal cone cell development and gene silencing by miRNA. KEGG pathway enrichment analysis did not identify any significantly associated pathways (*P*.adjust>0.05), but those that may be involved included phototransduction, arginine biosynthesis, and fructose and mannose metabolism. The top 10 associated KEGG pathways are displayed in Figure 5B.

A total of 3550, 2497, 2345, 2843, and 2255 circRNAs were predicted from 5 sequencing samples (Table 2). The circRNA expression in the different samples was detected using CIRI software, and a 97 differentially expressed circRNAs were identified using the R package DESeq. There were 49 upregulated circRNAs and 48 downregulated circRNAs.

Figure 6 includes statistics (Figure 6A) and cluster analysis (Figure 6B) for the differentially expressed circRNAs. GO enrichment analysis of all the genes (parental genes) from the differentially expressed circRNAs found that these genes were significantly associated ( $P_{\text{adjust}} < 0.05$ ) with 8 GO\_BP, 6 GO\_CC, and 2 GO\_MF terms; the top 10 GO terms associated with these genes are listed in Figure 7A. The GO\_BP terms associated with the parental genes included eye development, photoreceptor cell maintenance, visual perception and photoreceptor cell differentiation. KEGG pathway enrichment analysis did not identify any significantly associated pathways ( $p_{\text{adjust}} > 0.05$ ). The top 10 associated KEGG pathways are displayed in Figure 7B. Parental genes may be associated with the phosphatidylinositol pathway signaling system, glutamatergic synapses and EGFR tyrosine kinase inhibitor resistance. Finally, the target miRNAs of the differentially expressed circRNAs were predicted using miRanda software. We predicted 137 072 circRNA-miRNA regulatory relationships, including 1915 miRNAs and 97 differentially expressed RNAs.

A total of 59.77 M reads were obtained through miRNA library construction and sequencing, which included 95.97% miRNA reads, with an average of 1612 miRNAs identified in each sample. The differential expression analysis identified 84 differentially expressed, known miRNAs (including 42 upregulated and 42 downregulated) and 26 differentially expressed, novel miRNAs (including 7 upregulated and 19 downregulated; Figure 8). We predicted target genes for these known miRNAs and found that 83 miRNAs totaled 5039 target genes. These target genes were significantly correlated ( $P_{\text{adjust}} < 0.05$ ) with 957 GO\_BP, 145 GO\_CC, 124 GO\_MF terms (data not shown) and 40 KEGG pathways.

**Interaction Analysis and Network Map** As the method described, we further screened the interaction pairs of the differentially expressed mRNAs, lncRNAs, circRNAs and miRNAs and identified 359 circRNA-miRNA interaction relationships [ $\text{cor} < 0$  and  $P < 0.05$ ; including 51 differentially expressed circRNAs (16 upregulated circRNAs and 45 downregulated circRNA)] and 44 differentially expressed miRNAs (32 upregulated miRNAs and 12 downregulated miRNAs), 721 lncRNA-miRNA interaction relationships [ $\text{cor} < 0$  and  $P < 0.05$ ; including 366 differentially expressed lncRNAs (46 upregulated circRNAs and 320 downregulated circRNAs)] and 56 differentially expressed miRNAs (16 upregulated miRNAs and 40 downregulated miRNAs). We did not find any significant miRNA-mRNA relationship pairs; none of the relationship pairs met the  $P > 0.05$  threshold. Prediction of lncRNA-mRNA interaction pairs (cis and trans) showed that there were 475 425 cis lncRNA-mRNA pairs, including 289 565 positively regulated cis lncRNA-mRNA relationship

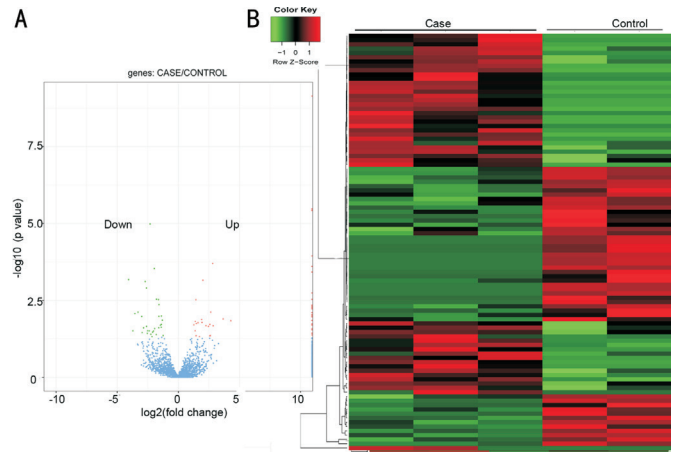


**Figure 6** Volcano plot and hierarchical clustering of differentially expressed circRNAs A: Volcano plot. Green and red nodes indicate down [ $\log_2(\text{fold change}) < -1$ ,  $P < 0.05$ ] and upregulated circRNAs [ $\log_2(\text{fold change}) > 1$ ,  $P < 0.05$ ], respectively. Blue color represents nondifferentially expressed lncRNAs. B: Heatmap analysis of differentially expressed circRNAs. Red and green color denotes up and downregulated expression profiles in samples, respectively.

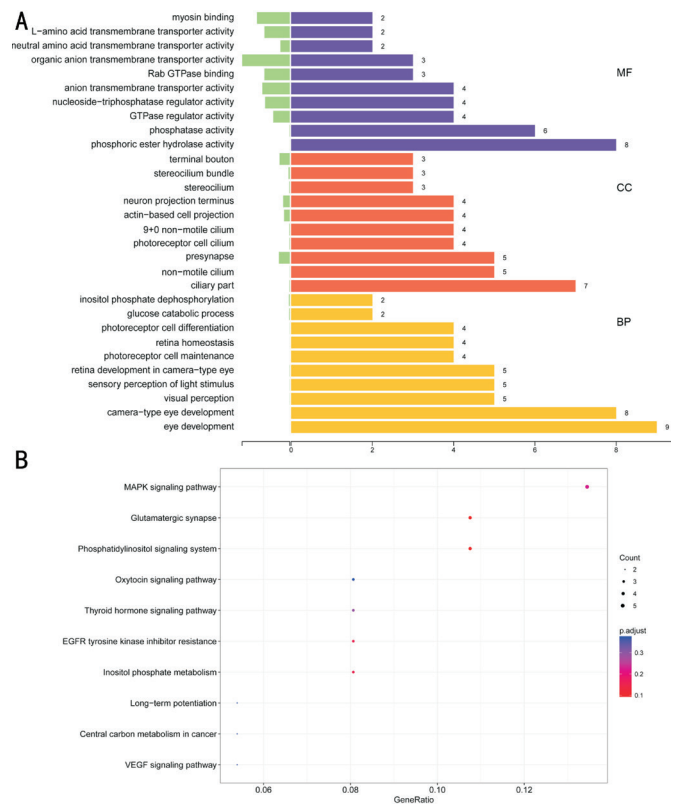


**Figure 7** The GO terms and KEGG pathways associated with parental genes of differentially expressed circRNAs in the case sample compared with the control A: Top 30 GO terms. Ten categories are listed for each classification; B: Top 10 KEGG pathways. Bubble size represents gene number. Bubble color indicates P.adjust value. MF: Molecular function; CC: Cellular component; BP: Biological process.

pairs [ $\text{cor} > 0$  and  $P < 0.05$ ; including 4233 differentially expressed lncRNAs (2439 upregulated lncRNAs and 1794 downregulated lncRNAs)] and 738 differentially expressed

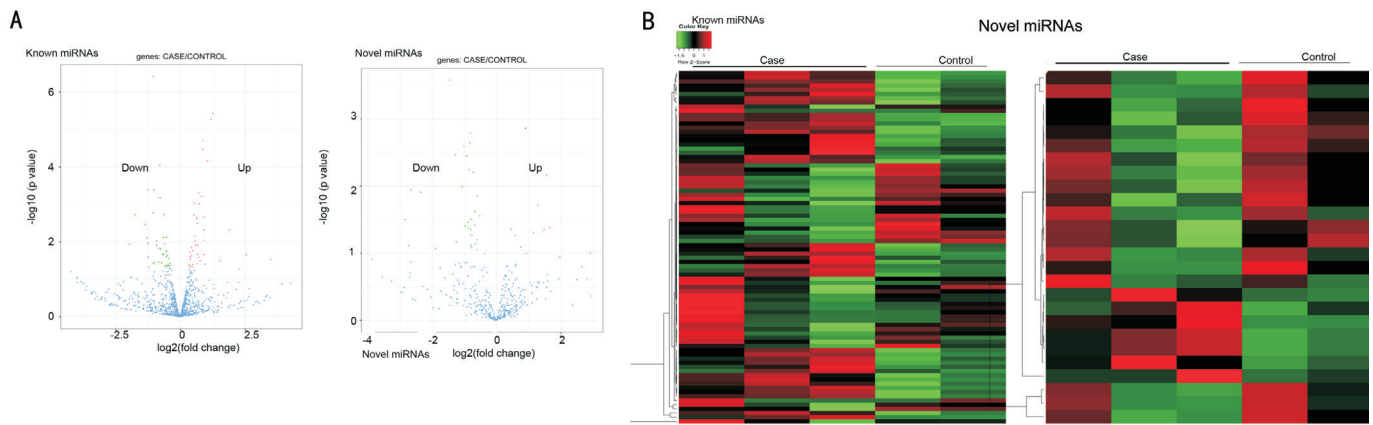


**Figure 8 Volcano plot and hierarchical clustering of differentially expressed miRNAs** A: Volcano plot of the differentially expressed known and novel miRNAs. Green and red nodes indicate down [ $\log_2(\text{fold change}) < -1$ ,  $P < 0.05$ ] and upregulated miRNAs [ $\log_2(\text{fold change}) > 1$ ,  $P < 0.05$ ], respectively. Blue color represents nondifferentially expressed miRNAs. B: Heatmap analysis of the differentially expressed known and novel miRNAs. Red and green color denotes up and downregulated expression profiles in the samples, respectively.

mRNAs (431 upregulated mRNAs and 307 downregulated mRNA). The lncRNA trans regulatory results were the same as the cis results.

**lncRNA ceRNA and circRNA ceRNA network map** To construct a ceRNA network map, we utilized 289 565 pairs of positive lncRNA-mRNA expression, including 197 differentially expressed genes and 4232 differentially expressed lncRNAs, and identified 162 differentially expressed miRNAs that had a defined relationship with the pairs. The lncRNA-miRNA-mRNA ceRNA network map was constructed using Cytoscape software, and was composed of 1593 ceRNAs and 1029 nodes, which included 17 differentially expressed miRNAs, 36 differentially expressed genes, and 976 differentially expressed lncRNAs. To identify ceRNAs that had the greatest likelihood of myopia, we used the 5 differentially expressed miRNAs with the most interactions (including 4 upregulated mRNA, mmu-miR-34a-5p, mmu-miR-339-5p, mmu-miR-298-5p and mmu-miR-320-3p, and 1 downregulated mRNA, mmu-miR-485-5p)

The network includes 22 differentially expressed genes (downregulated genes included TGM3, HCLS1, PNPLA3 and IGSF9; upregulated genes included CANT1, Fos, GADD45B, Foxi1, TREM2, Oas1a, Oas1h, IRF7, OLFM2 and Myo10). Each miRNA was regulated by 1-3 differentially expressed lncRNAs (Figure 9). Examples include upregulated OLFM2/Myo10 (up)-mmu-miR-320-3p (up)-A830012C17Rik/Gm20426/NONMMUG002837.2 (up), Fos (up)- mmu-miR-34a-5p (up)-4930573C15Rik (up), and Bcl3 (up)- mmu-miR-298-5p (up)- Gm662/4930542C16Rik/Gm26538 (up), Foxi1/Oas1h/IRF7 (up)- mmu-miR-298-5p (up)- 1700030A11Rik/Gm11131/Gm11725/Gm16565/NONMMUG025971.2 (up), Oas1a (up)- mmu-miR-485-5p (down)-Gm14205/Gm11131 (up), Gadd45b (up)- mmu-

miR-485-5p (down) -Gm16174/Gm28703/Ttc39aos1 (up) of ceRNA *etc.*; and the downregulated TGM3 (down)- mmu-miR-339-5p (up)- 4930405A21Rik/Dbhos/Gm11961/NONMMUG036959.1/NONMMUG043173.2/NONMMUG005330.1 (down), IGSF9 (down)- mmu-miR-34a-5p (up)-4930405A21Rik (down), HCLS1 (down)- mmu-miR-298-5p (up)- NONMMUG036959.1/NONMMUG043173.2/NONMMUG005330.1 (down) or ceRNA of PNPLA3 (down)- mmu-miR-298-5p (up)- NONMMUG043173.2/NONMMUG005330.1 (down) *etc.*

Similarly, a ceRNA was constructed using the 359 identified circRNA-miRNA interaction pairs [including 51 differentially expressed circRNAs (16 upregulated circRNAs and 45 downregulated circRNAs)], with the obtained circRNA-miRNA-mRNA ceRNA including 35 differentially expressed genes, 54 circRNAs and 9 miRNAs for a total of 239 ceRNAs. We continued to focus on the top 5 differentially expressed miRNAs with the most interactions and used these interactions to compose the ceRNA network (Figure 10). The ceRNA network that we generated included 22 differentially expressed genes (including upregulated FOXI1, OAS1A, GADD45B, TREM2, IRF7, OLFM2 and Myo10, and downregulated PNPLA3, IGSF9, TGM3, GUCA1B and HCLS1). Other examples include TGM3 (down)- mmu-miR-103-3p (up)- Eif4g3/Herc3/Cpeb3/Rims2 derived circRNAs (down; here you can change to circRNA sites), GUCA1B (down)- mmu-miR-145-5p (up)- Eif4g3/Herc3/Cpeb3/Rims2 derived circRNAs (down), HCLS1/PNPLA3 (down)- mmu-miR-298-5p (up)- Herc3/Cpeb3/Rims2 derived circRNAs (down), Gadd45b (up)-mmu-miR-485-5p (down)- Papd7/Slit2/Inpp4b derived circRNAs (up), OAS1A (up)-mmu-miR-485-5p (down)-Slit2/Prdm5/Zfhx4/Zzef1 (up), IRF7 (up)- mmu-miR-298-5p (up)- Slit2/Prdm5/Zfhx4/Zzef1 (up) ceRNA.

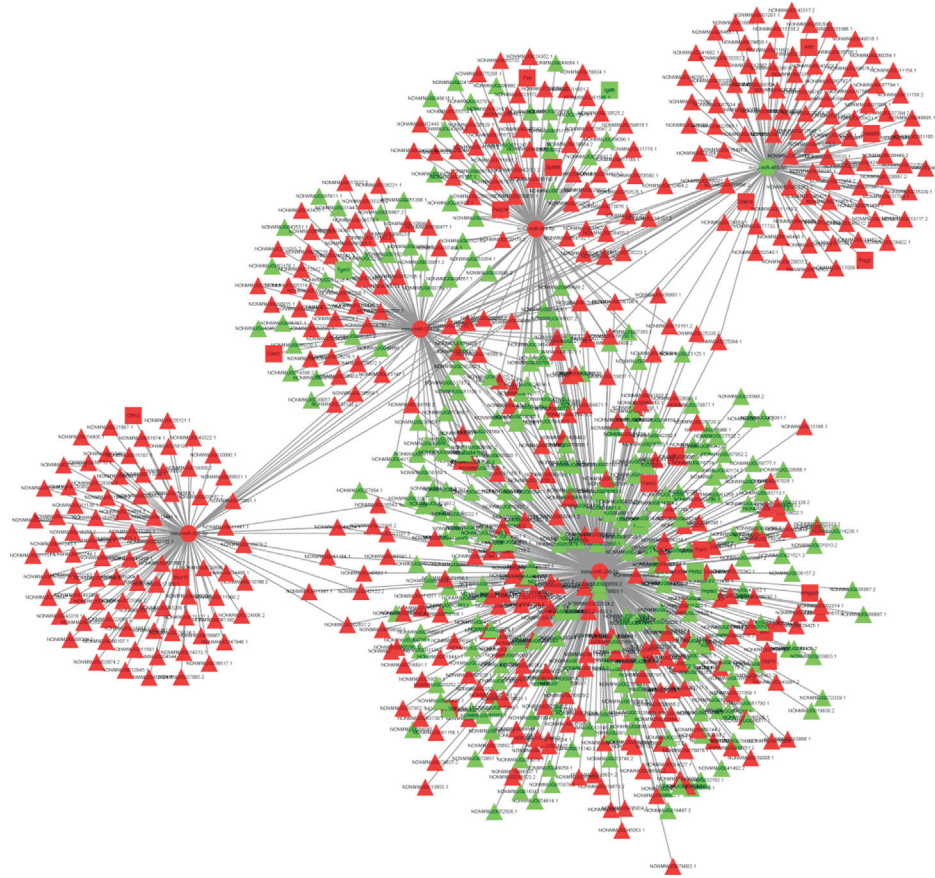


**Figure 9** The lncRNA-miRNA-mRNA ceRNA network for the 5 miRNAs with the highest number of interactions. Red and green color represent up- and down-regulation in the case sample compared with the control. Circles, triangles, and squares indicate differentially expressed miRNAs, lncRNAs and mRNAs (gene), respectively.

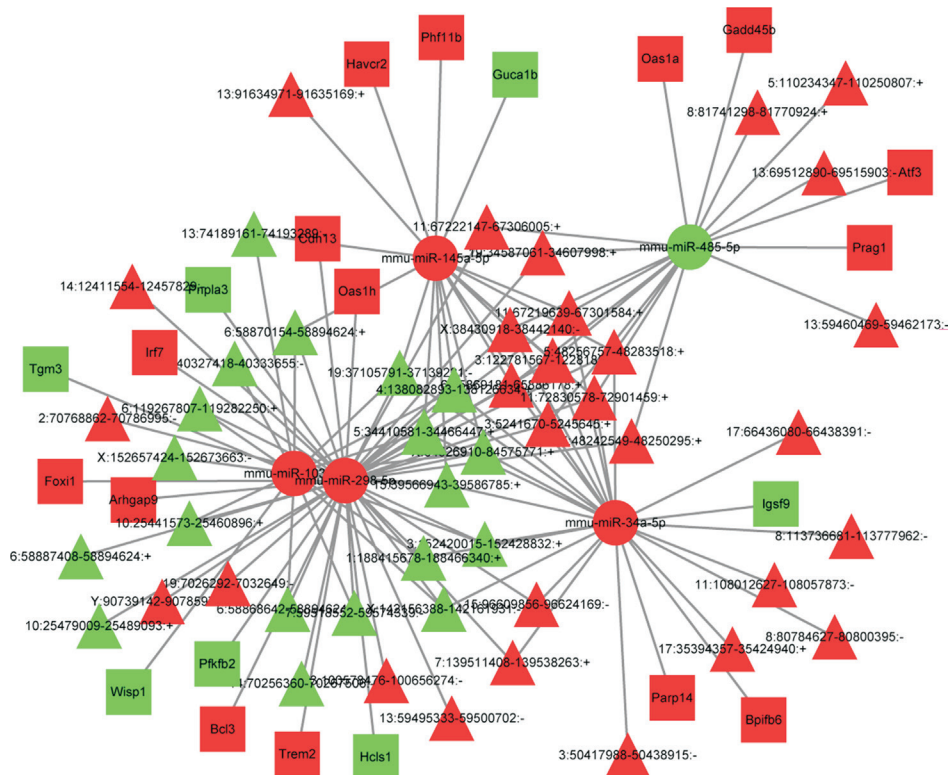


**Figure 10** The circRNA-miRNA-mRNA ceRNA network of the 5 miRNAs with the highest number of interactions. Red and green color represent up- and down-regulation in the case sample compared with the control. Circles, triangles, and squares indicate differentially expressed miRNAs, lncRNAs and mRNAs (gene), respectively.

## DISCUSSION

Blue light is abundantly present in low intensity display devices, such as mobile phones, display screens, LEDs and other lights<sup>[48-49]</sup>. The use of display devices with low intensity blue light has become increasingly popular in the present day<sup>[50-51]</sup>. The retina is the main target tissue of blue light damage in terrestrial animals, and the long exposure time to high energy blue light causes eye diseases through photosensitization and other oxygen-dependent processes. However, very little is known about the relationship between genetic background, gene expression and blue light damage.

In our study, whole mouse eyeballs were used and a relatively large number and diversity of gene expression changes were recorded. Our data present both a theoretical and experimental study of the blue light damage to eyeballs. We performed RNA-seq analysis to reveal the transcriptional changes and key signaling pathways affected by blue light. Our data suggested that differences in gene expression played a very important role in blue light damage. Genes that were involved in blue light damage in the eyeball composed a long list of biological and MFs, which suggests that blue light damage is associated with specific patterns of gene expression and the activation or suppression of many eye signaling pathways.

In this study, we identified 737 differentially expressed genes, including 430 upregulated genes and 307 downregulated genes. Our data indicated that exposure to blue light can cause a certain degree of abnormal gene expression in the body. Gene ontology analysis revealed that the 737 genes whose expression correlated with blue light damage were associated with 425 BP, 29 CC, and 39 MF. Genes that we found to be involved in blue light damage in mice affected a multitude of BP in eyes, such as visual perception and sensory perception of light stimulus. Our recent study has shown that exposure to blue light can cause a significant increase in the expression of *OLFACTOMEDIN2* (*OLFM2*), *SMAD2* and *SMAD3*. Previous studies have shown that *OLFM2* expression was *SMAD2/3*-dependent and the expression of the *OLFM2* gene correlated with human ocular anomalies and eye diseases, including anophthalmia, microphthalmia and coloboma<sup>[52-53]</sup>. *Olfm2* plays an important role in mammalian eye development and visual perception. Some data have suggested that *GUCA1B* gene mutation causes one form of autosomal retinal dystrophy and retinal degeneration<sup>[54-57]</sup> and affects the retina's sensory perception of light stimulus. An experimental study on blue light-induced oxidative stress injury on mouse retinas showed that blue light induced a decrease in visual function that correlated with photoreceptor morphological changes<sup>[58-61]</sup>. Periodic blue light exposure caused atrophy of photoreceptors and injured neuron transduction in the retina. Exposure to constant blue light considerably reduced the visual responses

and reduced the functional loss of retinal photosensitive cells<sup>[62]</sup>. Mouse retinas became disordered in the inner and outer segments of the photoreceptor cells when compared with the normal control group after exposure to blue light<sup>[63]</sup>. Our data showed that the cell composition of the photoreceptor outer segment, the photoreceptor cell cilium, and non-motile cilium were significantly correlated with blue light damage. This is consistent with previous reports. Additionally, we found that MFs including cytokine receptor activity, G-protein coupled receptor binding, CCR chemokine receptor binding and T cell receptor binding strongly correlated with blue light damage on the eyeballs.

Most noteworthy is the finding that 39 KEGG pathways were involved blue light damage to the eyeball, including phototransduction, the JAK-STAT signaling pathway, cytokine-cytokine receptor interactions and several pathways related to viruses or bacteria (including herpes simplex infection, *Staphylococcus aureus* infection and *Epstein-Barr* virus infection). Analysis of the main KEGG results revealed that the pathways involved in cell apoptosis and the response to oxidative stress were among the most influenced. Phototransduction takes place in the rod and cone photoreceptor cells and it is involved in the progress of light-triggered electrical signals<sup>[64-66]</sup>. Previous data also suggested that the phototransduction pathway could reverse hyperopia in refractive eye development after blue light irradiation<sup>[67-68]</sup>, which could help to explain why phototransduction was activated after blue light exposure. Some studies indicated that *Guca1b* encoding GCAP1 protein plays an important role in phototransduction by activating Ret-GC1<sup>[69]</sup>.

Previous studies showed that Müller cells mediated inner retinal osmohomeostasis and displayed hypertrophy after blue light treatment<sup>[70]</sup>. The JAK-STAT signaling pathway can regulate the proliferation and differentiation of Müller cells and further regulates retinal cell apoptosis<sup>[71-73]</sup>. In our study, JAK-STAT signaling pathways were activated under blue light treatment, which suggested that blue light induced Müller cell apoptosis through JAK-STAT signaling pathways.

Genes that we found to be involved in refractive error development in mice affected a multitude of biological functions in the eyeball. For example, we found that mutations in the *SMAD3* gene were involved in the regulation of scleral remodeling by the TGF- $\beta$ /smad pathway<sup>[74]</sup>. Mutations in *OLFM2* were found to be associated with intraocular hypertension and development of retinal ganglion cells<sup>[53]</sup>. Taken together, these data suggest that blue-light damage to the eyeball is a complicated process that is regulated by a large number of pathways.

Our study also analyzed the association of miRNAs and target genes with lncRNAs and circRNAs. Genetic data suggested

that miR-34a-5p was related to the oxidative stress response<sup>[75]</sup>. Expression of miR-485-5p was regulated by Gadd45b and suppressed cell migration and invasion<sup>[76]</sup>. We analyzed 5 differentially expressed miRNAs (including mmu-miR-34a-5p, mmu-miR-339-5p, mmu-miR-298-5p and mmu-miR-320-3p). Their relationship was regulated by multiple lncRNAs and circRNAs, such as Gadd45b (up)-mmu-miR-485-5p (down)- Papd7/Slit2/Inpp4b derived circRNAs (up). The results indicated that the mechanism of blue light damage was complicated and regulated by many ceRNAs.

Although there are important discoveries revealed by these studies, there are also limitations. In our study, we analyzed data from 3 pairs of eyes, and because of the small sample size, we may have underestimated the actual changes. The accuracy of our data needs to be further studied. In summary, we have identified a certain extent of the blue light damage to eyeballs at the genetic level. Gene expression changes led to changes in the gene balance and signaling pathway expression. These findings improve our understanding of the global genetic responses to blue light exposure in the mouse eye and offer a new strategy and theoretical basis to treat eye diseases by gene therapy.

In conclusion, we have identified that blue light damage is associated with specific patterns of gene expression and the activation or suppression of eye signaling pathways. A certain level of blue light can cause damage to eyeball at the genetic level. These results thus offer a new strategy and theoretical basis to treat eye diseases by gene therapy.

#### ACKNOWLEDGEMENTS

**Foundations:** Supported by the National Natural Science Foundation of China (No.11802209); the Natural Science Foundation of Shandong Province China (No.ZR2019MA018; No.ZR2019BC095); Shandong Project for Talents Introduction and Development on Youth Innovation Team of Higher Education.

**Conflicts of Interest:** Ouyang XL, None; Chen BY, None; Xie YF, None; Wu YD, None; Guo SJ, None; Dong XY, None; Wang GH, None.

#### REFERENCES

- 1 Krigel A, Berdugo M, Picard E, Levy-Boukris R, Jaadane I, Jonet L, Dernigoghossian M, Andrieu-Soler C, Torriglia A, Behar-Cohen F. Light-induced retinal damage using different light sources, protocols and rat strains reveals LED phototoxicity. *Neuroscience* 2016;339:296-307.
- 2 Algvare PV, Marshall J, Seregard S. Age-related maculopathy and the impact of blue light hazard. *Acta Ophthalmol Scand* 2006;84(1):4-15.
- 3 Zhao ZC, Zhou Y, Tan G, Li J. Research progress about the effect and prevention of blue light on eyes. *Int J Ophthalmol* 2018;11(12):1999-2003.
- 4 Niwano Y, Kanno T, Iwasawa A, Ayaki M, Tsubota K. Blue light injures corneal epithelial cells in the mitotic phase *in vitro*. *Br J Ophthalmol* 2014;98(7):990-992.

- 5 Rózanowska M, Jarvis-Evans J, Korytowski W, Boulton ME, Burke JM, Sarna T. Blue light-induced reactivity of retinal age pigment. *In vitro* generation of oxygen-reactive species. *J Biol Chem* 1995;270(32):18825-18830.
- 6 Kaido M, Toda I, Oobayashi T, Kawashima M, Katada Y, Tsubota K. Reducing short-wavelength blue light in dry eye patients with unstable tear film improves performance on tests of visual acuity. *PLoS One* 2016;11(4):e0152936.
- 7 Lee HS, Cui L, Li Y, Choi JS, Choi JH, Li ZR, Kim GE, Choi W, Yoon KC. Influence of light emitting diode-derived blue light overexposure on mouse ocular surface. *PLoS One* 2016;11(8):e0161041.
- 8 Lee SI, Matsumori K, Nishimura K, Nishimura Y, Ikeda Y, Eto T, Higuchi S. Melatonin suppression and sleepiness in children exposed to blue-enriched white LED lighting at night. *Physiol Rep* 2018;6(24):e13942.
- 9 Motamedzadeh M, Golmohammadi R, Kazemi R, Heidarimoghadam R. The effect of blue-enriched white light on cognitive performances and sleepiness of night-shift workers: a field study. *Physiol Behav* 2017;177:208-214.
- 10 van der Maren S, Moderie C, Duclos C, Paquet J, Daneault V, Dumont M. Daily profiles of light exposure and evening use of light-emitting devices in young adults complaining of a delayed sleep schedule. *J Biol Rhythm* 2018;33(2):192-202.
- 11 West KE, Jablonski MR, Warfield B, Cecil KS, James M, Ayers MA, Maida J, Bowen C, Sliney DH, Rollag MD, Hanifin JP, Brainard GC. Blue light from light-emitting diodes elicits a dose-dependent suppression of melatonin in humans. *J Appl Physiol* 2011;110(3):619-626.
- 12 Wu JM, Seregard S, Algvare PV. Photochemical damage of the retina. *Surv Ophthalmol* 2006;51(5):461-481.
- 13 Tosini G, Ferguson I, Tsubota K. Effects of blue light on the circadian system and eye physiology. *Mol Vis* 2016;22:61-72.
- 14 Narimatsu T, Ozawa Y, Miyake S, Kubota S, Yuki K, Nagai N, Tsubota K. Biological effects of blocking blue and other visible light on the mouse retina. *Clin Exp Ophthalmol* 2014;42(6):555-563.
- 15 Ratnayake K, Payton JL, Lakmal OH, Karunarathne A. Blue light excited retinal intercepts cellular signaling. *Sci Rep* 2018;8(1):10207.
- 16 Vicente-Tejedor J, Marchena M, Ramírez L, García-Ayuso D, Gómez-Vicente V, Sánchez-Ramos C, de la Villa P, Germain F. Removal of the blue component of light significantly decreases retinal damage after high intensity exposure. *PLoS One* 2018;13(3):e0194218.
- 17 Pang J, Seko Y, Tokoro T. Processes of blue light-induced damage to retinal pigment epithelial cells lacking phagosomes. *Jpn J Ophthalmol* 1999;43(2):103-108.
- 18 Li JY, Zhang K, Xu D, Zhou WT, Fang WQ, Wan YY, Yan DD, Guo MY, Tao JX, Zhou WC, Yang F, Jiang LP, Han XJ. Mitochondrial fission is required for blue light-induced apoptosis and mitophagy in retinal neuronal R28 cells. *Front Mol Neurosci* 2018;11:432.
- 19 Moon J, Yun J, Yoon YD, *et al*. Blue light effect on retinal pigment epithelial cells by display devices. *Integr Biol (Camb)* 2017;9(5):436-443.

- 20 Marek V, Mélik-Parsadaniantz S, Villette T, Montoya F, Baudouin C, Brignole-Baudouin F, Denoyer A. Blue light phototoxicity toward human corneal and conjunctival epithelial cells in basal and hyperosmolar conditions. *Free Radic Biol Med* 2018;126:27-40.
- 21 Yan GG, Zhang L, Feng C, et al. Blue light emitting diodes irradiation causes cell death in colorectal cancer by inducing ROS production and DNA damage. *Int J Biochem Cell Biol* 2018;103:81-88.
- 22 Tao JX, Zhou WC, Zhu XG. Mitochondria as potential targets and initiators of the blue light hazard to the retina. *Oxid Med Cell Longev* 2019;2019:6435364.
- 23 Núñez-Álvarez C, Osborne NN. Blue light exacerbates and red light counteracts negative insults to retinal ganglion cells *in situ* and R28 cells *in vitro*. *Neurochem Int* 2019;125:187-196.
- 24 Osborne NN, Núñez-Álvarez C, Del Olmo-Aguado S, Merrayo-Lloves J. Visual light effects on mitochondria: the potential implications in relation to glaucoma. *Mitochondrion* 2017;36:29-35.
- 25 Lin CH, Wu MR, Li CH, Cheng HW, Huang SH, Tsai CH, Lin FL, Ho JD, Kang JJ, Hsiao G, Cheng YW. Editor's highlight: periodic exposure to smartphone-mimic low-luminance blue light induces retina damage through bcl-2/BAX-dependent apoptosis. *Toxicol Sci* 2017;157(1):196-210.
- 26 Sparrow JR, Zhou JL, Cai BL. DNA is a target of the photodynamic effects elicited in A2E-laden RPE by blue-light illumination. *Invest Ophthalmol Vis Sci* 2003;44(5):2245-2251.
- 27 Sparrow JR, Nakanishi K, Parish CA. The lipofuscin fluorophore A2E mediates blue light-induced damage to retinal pigmented epithelial cells. *Invest Ophthalmol Vis Sci* 2000;41(7):1981-1989.
- 28 Sparrow JR, Cai B. Blue light-induced apoptosis of A2E-containing RPE: involvement of caspase-3 and protection by Bcl-2. *Invest Ophthalmol Vis Sci* 2001;42(6):1356-1362.
- 29 Sparrow JR, Zhou JL, Ben-Shabat S, Vollmer H, Itagaki Y, Nakanishi K. Involvement of oxidative mechanisms in blue-light-induced damage to A2E-laden RPE. *Invest Ophthalmol Vis Sci* 2002;43(4):1222-1227.
- 30 Kim D, Langmead B, Salzberg SL. HISAT: a fast spliced aligner with low memory requirements. *Nat Methods* 2015;12(4):357-360.
- 31 DeLuca DS, Levin JZ, Sivachenko A, Fennell T, Nazaire MD, Williams C, Reich M, Winckler W, Getz G. RNA-SeQC: RNA-seq metrics for quality control and process optimization. *Bioinformatics* 2012;28(11):1530-1532.
- 32 Shen SH, Park JW, Lu ZX, Lin L, Henry MD, Wu YN, Zhou Q, Xing Y. rMATS: robust and flexible detection of differential alternative splicing from replicate RNA-Seq data. *Proc Natl Acad Sci U S A* 2014;111(51):E5593-E5601.
- 33 Trapnell C, Roberts A, Goff L, Pertea G, Kim D, Kelley DR, Pimentel H, Salzberg SL, Rinn JL, Pachter L. Differential gene and transcript expression analysis of RNA-seq experiments with TopHat and cufflinks. *Nat Protoc* 2012;7(3):562-578.
- 34 Kanehisa M, Araki M, Goto S, Masahiro H, Mika H, Masumi I, Toshiaki K, Shuichi K, Shujiro O, Toshiaki T, Yoshihiro Y. KEGG for linking genomes to life and the environment. *Nucleic Acids Res* 2008;36:480-484.
- 35 Li JW, Ma W, Zeng P, Wang JY, Geng B, Yang JC, Cui QH. LncTar: a tool for predicting the RNA targets of long noncoding RNAs. *Brief Bioinformatics* 2015;16(5):806-812.
- 36 Gao Y, Wang JF, Zhao FQ. CIRI: an efficient and unbiased algorithm for de novo circular RNA identification. *Genome Biol* 2015;16:4.
- 37 Love MI, Huber W, Anders S. Moderated estimation of fold change and dispersion for RNA-seq data with DESeq2. *Genome Biol* 2014;15(12):550.
- 38 Anders S, Huber W. Differential expression analysis for sequence count data. *Genome Biol* 2010;11(10):R106.
- 39 Enright AJ, John B, Gaul U, Tuschl T, Sander C, Marks DS. MicroRNA targets in Drosophila. *Genome Biol* 2003;5(1):R1.
- 40 Kozomara A, Griffiths-Jones S. miRBase: integrating microRNA annotation and deep-sequencing data. *Nucleic Acids Res* 2011;39(Database issue):D152-D157.
- 41 Griffiths-Jones S, Grocock RJ, van Dongen S, Bateman A, Enright AJ. miRBase: microRNA sequences, targets and gene nomenclature. *Nucleic Acids Res* 2006;34(Database issue):D140-D144.
- 42 Griffiths-Jones S, Saini HK, van Dongen S, Enright AJ. miRBase: tools for microRNA genomics. *Nucleic Acids Res* 2008;36(Database issue):D154-D158.
- 43 Kozomara A, Griffiths-Jones S. miRBase: annotating high confidence microRNAs using deep sequencing data. *Nucleic Acids Res* 2014;42(Database issue):D68-D73.
- 44 Griffiths-Jones S, Bateman A, Marshall M, Khanna A, Eddy SR. Rfam: an RNA family database. *Nucleic Acids Res* 2003;31(1):439-441.
- 45 Friedländer MR, Chen W, Adamidi C, Maaskola J, Einspanier R, Knespel S, Rajewsky N. Discovering microRNAs from deep sequencing data using miRDeep. *Nat Biotechnol* 2008;26(4):407-415.
- 46 Betel D, Wilson M, Gabow A, Marks DS, Sander C. The microRNA.org resource: targets and expression. *Nucleic Acids Res* 2008;36(Database issue):D149-D153.
- 47 Rehmsmeier M, Steffen P, Hochsmann M, Giegerich R. Fast and effective prediction of microRNA/target duplexes. *RNA* 2004;10(10):1507-1517.
- 48 Marshall J. Light in man's environment. *Eye (Lond)* 2016;30(2):211-214.
- 49 Lin CW, Yang CM, Yang CH. Effects of the emitted light spectrum of liquid crystal displays on light-induced retinal photoreceptor cell damage. *Int J Mol Sci* 2019;20(9):E2318.
- 50 O'Hagan JB, Khazova M, Price LL. Low-energy light bulbs, computers, tablets and the blue light hazard. *Eye (Lond)* 2016;30(2):230-233.
- 51 Bullough JD, Bierman A, Rea MS. Evaluating the blue-light hazard from solid state lighting. *Int J Occup Saf Ergon* 2019;25(2):311-320.
- 52 Shi N, Guo X, Chen SY. Olfactomedin 2, a novel regulator for transforming growth factor- $\beta$ -induced smooth muscle differentiation of human embryonic stem cell-derived mesenchymal cells. *Mol Biol Cell* 2014;25(25):4106-4114.

- 53 Shi N, Chen SY. From nerve to blood vessel: a new role of Olfm2 in smooth muscle differentiation from human embryonic stem cell-derived mesenchymal cells. *J Biomed Res* 2015;29(4):261-263.
- 54 Sato M, Nakazawa M, Usui T, Tanimoto N, Abe H, Ohguro H. Mutations in the gene coding for guanylate cyclase-activating protein 2 (GUCA1B gene) in patients with autosomal dominant retinal dystrophies. *Graefes Arch Clin Exp Ophthalmol* 2005;243(3):235-242.
- 55 Kitaritschky VB, Glöckner CJ, Kohl S. Mutation screening of the GUCA1B gene in patients with autosomal dominant cone and cone rod dystrophy. *Ophthalmic Genet* 2011;32(3):151-155.
- 56 Zhang QJ, Li W, Xiao XS, Li SQ, Guo XM. Analysis of GUCA1B, GNGT1 and RGS9 genes in patients with retinitis pigmentosa. *Hereditas* 2002;24(1):19-21.
- 57 Makino CL, Peshenko IV, Wen XH, Olshevskaya EV, Barrett R, Dizhoor AM. A role for GCAP2 in regulating the photoresponse. Guanylyl cyclase activation and rod electrophysiology in GUCA1B knock-out mice. *J Biol Chem* 2008;283(43):29135-29143.
- 58 Hall H, Ma JQ, Shekhar S, Leon-Salas WD, Weake VM. Blue light induces a neuroprotective gene expression program in Drosophila photoreceptors. *BMC Neurosci* 2018;19(1):43.
- 59 Ooe E, Tsuruma K, Kuse Y, Kobayashi S, Shimazawa M, Hara H. The involvement of ATF<sub>4</sub> and S-opsin in retinal photoreceptor cell damage induced by blue LED light. *Mol Vis* 2017;23:52-59.
- 60 Chen WJ, Wu CY, Xu ZH, Kuse Y, Hara H, Duh EJ. Nrf2 protects photoreceptor cells from photo-oxidative stress induced by blue light. *Exp Eye Res* 2017;154:151-158.
- 61 Kuse Y, Ogawa K, Tsuruma K, Shimazawa M, Hara H. Damage of photoreceptor-derived cells in culture induced by light emitting diode-derived blue light. *Sci Rep* 2014;4:5223.
- 62 Léveillard T, Sahel JA. Metabolic and redox signaling in the retina. *Cell Mol Life Sci* 2017;74(20):3649-3665.
- 63 Liu Q, Zhang Q, Pierce EA. Photoreceptor sensory cilia and inherited retinal degeneration. *Adv Exp Med Biol* 2010;664:223-232.
- 64 Detwiler PB. Phototransduction in retinal ganglion cells. *Yale J Biol Med* 2018;91(1):49-52.
- 65 Fu YB, Yau KW. Phototransduction in mouse rods and cones. *Pflügers Arch-Eur J Physiol* 2007;454(5):805-819.
- 66 Saless C. Physiology of the visual retinal signal: from phototransduction to the visual cycle. *J Fr Ophtalmol* 2017;40(3):239-250.
- 67 Lamb TD, Hunt DM. Evolution of the calcium feedback steps of vertebrate phototransduction. *Open Biol* 2018;8(9):180119.
- 68 Lamb TD. Evolution of phototransduction, vertebrate photoreceptors and retina. *Prog Retin Eye Res* 2013;36:52-119.
- 69 Payne AM, Downes SM, Bessant DA, Plant C, Moore T, Bird AC, Bhattacharya SS. Genetic analysis of the guanylate cyclase activator 1B (GUCA1B) gene in patients with autosomal dominant retinal dystrophies. *J Med Genet* 1999;36(9):691-693.
- 70 Iandiev I, Wurm A, Hollborn M, Wiedemann P, Grimm C, Remé CE, Reichenbach A, Pannicke T, Bringmann A. Müller cell response to blue light injury of the rat retina. *Invest Ophthalmol Vis Sci* 2008;49(8):3559-3567.
- 71 Todd L, Squires N, Suarez L, Fischer AJ. Jak/Stat signaling regulates the proliferation and neurogenic potential of Müller glia-derived progenitor cells in the avian retina. *Sci Rep* 2016;6:35703.
- 72 Lozano DC, Choe TE, Cepurna WO, Morrison JC, Johnson EC. Early optic nerve head glial proliferation and jak-stat pathway activation in chronic experimental glaucoma. *Invest Ophthalmol Vis Sci* 2019;60(4):921-932.
- 73 Vigneswara V, Akpan N, Berry M, Logan A, Troy CM, Ahmed Z. Combined suppression of CASP<sub>2</sub> and CASP<sub>6</sub> protects retinal ganglion cells from apoptosis and promotes axon regeneration through CNTF-mediated JAK/STAT signalling. *Brain* 2014;137(Pt 6):1656-1675.
- 74 Qing J, Liu C, Choy L, Wu RY, Pagano JS, Derynck R. Transforming growth factor beta/Smad3 signaling regulates IRF-7 function and transcriptional activation of the beta interferon promoter. *Mol Cell Biol* 2004;24(3):1411-1425.
- 75 Wan Y, Cui RX, Gu JX, Zhang X, Xiang XH, Liu C, Qu K, Lin T. Identification of four oxidative stress-responsive microRNAs, miR-34a-5p, miR-1915-3p, miR-638, and miR-150-3p, in hepatocellular carcinoma. *Oxid Med Cell Longev* 2017;2017: 5189138.
- 76 Lou C, Xiao M, Cheng S, Lu X, Jia S, Ren Y, Li Z. MiR-485-3p and miR-485-5p suppress breast cancer cell metastasis by inhibiting PGC-1 $\alpha$  expression. *Cell Death Dis* 2016;7(3):e2159.